Analysing the land use/land cover influence on land surface temperature in San Luis Potosí Basin, México using remote sensing techniques

Analysing the land use/land cover influence on land surface temperature in San Luis Potosí Basin, México using remote sensing techniques

A G C Ovalle[1], A C Tristán[1*], J A Amador-Nieto[1], R F Putri[2*] and R A Zahra[2]

[1]Geomatics Engineering, Faculty of Engineering, Autonomous University of San Luis Potosí, México.
[2]Department of Environmental Geography, Faculty of Geography, Universitas Gadjah Mada, Indonesia.

[*] Corresponding author: abraham.cardenas@uaslp.mx, ratihfitria.putri@ugm.ac.id

Abstract. Changes in Land Use/Land Cover (LULC) generate several impacts which affect the energy balance of the Earth and, consequently, modifying the climate of a region. Accordingly, one of the most important indicators of this modification is the Land Surface Temperature (LST). The present work aims to analyze the relationship between LULC and LST, determining the influence of LULC on LST using Geographical Information Systems (GIS) and Remote Sensing (RS) techniques. The selected study area was the San Luis Potosí Basin, México (SLPB). A temporal analysis has been developed for 2007 and 2020. Satellite images from Landsat 5 TM and 8 OLI/TIRS has been used to calculate LST through a single-channel algorithm for winter and spring. LULC has been determined from a supervised classification with neural network algorithm. Finally, change rates for LULC and LST were assessed. The results indicate that an LST increase of 11 °C from 2007 to 2020 has been detected in the region. Also, results showed that covers with spare vegetation or without vegetation have the highest temperatures (29°C to 32°C). In comparison, the covers with dense vegetation and water showed the lowest temperatures (23°C to 25°C). This type of research allows addressing the LULC effects on LST, as well as prove its importance in improving land use planning systems.

1. Introduction

LST is a direct indicator of the temperature of the Earth surface, which can vary due to geological, geophysical and geochemical parameters of the Earth and atmosphere [1] [2]. It represents one of the most critical factors in climate change [3] and plays an essential role in several areas of study, such as LULC [4].

LULC changes significantly alter the balance of energy on the surface, causing variations in the climate of a region [5]. Therefore, when impervious surfaces replace vegetation cover on Earth, LST increases creating problems such as the change in evapotranspiration rates, modification of water and energy balance, and environmental impacts [6]. Thus, monitoring LULC and LST is vital to mitigate these impacts.

Nowadays, one of the principal methods replacing the use of information obtained from surface stations is the retrieval of LST through RS techniques. It has been demonstrated to be one of the preferred methods to analyze LST because a product with better spatial coverage can be obtained in near real-time [3]. For this purpose, several algorithms can be used to calculate LST, including the use of the single-channel algorithm to retrieve LST of products derived from Landsat satellites [1] [4] [7] [8]. In the same way, the use of images from Landsat satellites represents one of the most common alternatives for detecting changes in LULC [6] [7] [9]. Therefore, RS can be used to carry out studies at different spatial and temporal scales [7] in such a way that information can be useful for monitoring changes in LULC and LST and the relationship between these parameters can be established.

Developing this type of analysis allows establishing mitigation measures for the impacts of climate change, identifying changes associated with local activities [10]. In addition, these analyses can be useful for environmental protection and urban planning [11]. Accordingly, the main objective of this research is to analyze the LST variations based on its relationship with LULC using RS and GIS techniques. This research is vital to address the impacts caused to LST by LULC changes in San Luis Potosi Basin.

1.1. Study area

San Luis Potosí Basin (SLPB) is located in the State of San Luis Potosí, Mexico between parallels 22° 29' 41.85" to 21° 56' 48.29" N and meridians 101° 11' 15.49" to 100° 39' 7.83" W (Figure 1), covering an area of 1,786.78 km^2. SLPB belongs to the hydrological region of "El Saldo", which is one of the most important inland watersheds in the country. It is an endorheic semi-arid basin with torrential, temporary and intermittent runoff. The mountain ranges located at the west and southwest of the basin form its primary collector called "Río Santiago", which is regulated by the dams "El Peaje", "El Potosino" and "San José". These reservoirs provide water for domestic supply. Average annual precipitation of this area is 402.6 mm. The climate of SLPB is temperate with warm semi-arid summers and an average annual temperature of 17.5 °C [12].

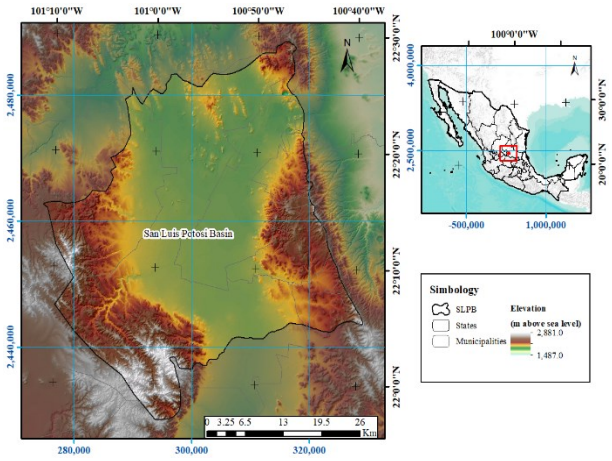

Figure 1. Location of the study area

2. Materials and Methods

2.1. Data

In order to accomplish the analysis, satellite images from Landsat 5 TM and Landsat 8 OLI/TIRS were obtained, available at the United States Geological Survey (USGS) website [13]. Dates, paths and rows used for the images are shown in table 1. Also, land use and vegetation map at a scale of 1: 250,000 was used, derived from series VI developed by the National Institute of Statistics and Geography (INEGI) [14].

Table 1. Satellite images used to obtain LST and LULC.

Path/Row	Sensor	Date
28/44	Landsat 5 TM	11-feb-07
28/44	Landsat 5 TM	18-may-07
28/45	Landsat 5 TM	11-feb-07
28/45	Landsat 5 TM	18-may-07
28/44	Landsat 8 OLI/TIRS	02-mar-20
28/44	Landsat 8 OLI/TIRS	21-may-20
28/45	Landsat 8 OLI/TIRS	02-mar-20
28/45	Landsat 8 OLI/TIRS	21-may-20

2.2. Image Processing – Correction

Performing a radiometric correction process to the satellite images was necessary to create high-quality data and to generate high-level processing products [15].

2.2.1. Conversion at-sensor spectral radiance

Convert the digital value of the pixel to calibrated radiance values is a fundamental step in radiometric calibration. This process ensures that data have a common and significant radiometric scale. For band 6 of Landsat 5 TM and band 10 of Landsat 8 OLI/TIRS, the method described by Chander *et al.* (2009) [15] was applied. Equation 1 shows the conversion of the original Digital Number (DN) to spectral radiance values.

$$L_\lambda = G_{rescale} \times Q_{cal} + B_{rescale} \qquad (1)$$

Where L_λ is the spectral radiance (W/m^2 sr μm); Q_{cal} is the DN of the pixel; $G_{rescale}$ and $B_{rescale}$ are band-specific rescaling factors of gains and bias from the sensor. Table 2 shows the values of $G_{rescale}$ and $B_{rescale}$ for the thermal bands used.

Table 2. Band-specific rescaling gain and bias factors [1] [15].

Band	Sensor	$G_{rescale}$	$B_{rescale}$
6	Landsat 5 TM	0.055376	1.18
10	Landsat 8 OLI/TIRS	0.0003342	0.1

2.2.2. Conversion to TOA reflectance

Conversion of DN to Top-of-Atmosphere (TOA) reflectance was performed using two different processes considering the sensor of interest. First, for Landsat 5 TM images, the methodology reported by Chander *et al.* (2009) [15] was applied. Equation 2 shows the conversion of spectral radiance values to TOA reflectance.

$$\rho_\lambda = \frac{\pi \times L_\lambda \times d^2}{ESUN_\lambda \times \cos\theta_s} \qquad (2)$$

Where ρ_λ is the TOA reflectance (dimensionless); π corresponds to the mathematical constant equal to ~3.14159 (dimensionless); L_λ is the spectral radiance (W/m^2 sr μm); d is the Earth-Sun distance (astronomic units); $ESUN_\lambda$ corresponds to the mean exoatmospheric solar irradiance (W/m^2 μm); θ_s is the solar zenith angle (radians). Values for d and $ESUN_\lambda$ were taken from Chander *et al.* (2009) [15].

Second, for Landsat 8 OLI/TIRS images, the original DN of bands 1-7 was converted to TOA reflectance values following Ariza (2013) [16]. Equation 3 shows the TOA reflectance conversion process.

$$\rho_\lambda = \frac{M_p \times Q_{cal} + A_p}{\sin \theta_{se}} \qquad (3)$$

Where M_p is the band-specific multiplicative rescaling factor; A_p is the band-specific additive rescaling factor; θ_{se} corresponds to the sun elevation angle (radians). Radiance scaling factors M_p (REFLECTANCE_MULT_BAND_x) and A_p (REFLECTANCE_ADD_BAND_x) are provided in the metadata file.

2.3. LST Retrieval

LST computation was performed in ENVI 5.3 software. A single-channel algorithm was applied following the process described by Mujabar (2019) [1]. First, the thermal band with spectral radiance values was converted to effective at-sensor brightness temperature (T_B, equation 4), according to Chander *et al.* (2009) [15]. T_B includes atmospheric effects such as absorption and emissions. This temperature assumes that the surface of the Earth is a black body [15].

$$T_B = \frac{K2}{\ln\left(\frac{K1}{L_\lambda} + 1\right)} \qquad (4)$$

Where T_B is effective at-sensor brightness temperature (°K); band 6 calibration constants (W/m^2 sr μm) are K1= 607.76 and K2 = 1260.56, whereas band 10 calibration constants are K1= 774.89 and K2 = 1321.08.

Once T_B is calculated, it is necessary to estimate the land surface emissivity, which is a crucial factor for LST retrieval. Land surface emissivity was calculated according to Mujabar (2019) [1], using the following equation:

$$\varepsilon = 0.973 - 0.047 \times P_V \qquad (5)$$

Where □□is the land surface emissivity (dimensionless); P_V is the Proportion of Vegetation (dimensionless). P_V can be calculated using equation 6, which involves the use of the Normalized Difference Vegetation Index (NDVI) [1].

$$Pv = \left(\frac{NDVI - NDVI_{min}}{NDVI_{max} - NDVI_{min}}\right)^2 \qquad (6)$$

Where NDVI (dimensionless, values from -1 to 1) can be obtained through equation 7 reported by Griend & Owe (1993) [17].

$$NDVI = \frac{\rho_{NIR} - \rho_{RED}}{\rho_{NIR} + \rho_{RED}} \qquad (7)$$

Finally, LST was calculated using equation 8 according to Mujabar (2019) [1].

$$LST = \frac{T_B}{\left[1 + \left(\lambda \times \frac{T_B}{\rho} \times \ln \varepsilon\right)\right]} \qquad (8)$$

Where T_B corresponds to effective at-sensor brightness temperature (°K); □□is the central wavelength of the emitted radiance (band 6, □ = 11.435 μm; band 10, □ = 10.895 μm); □ is a constant equal to 14,380 μmK (□□=h × c/σ, where σ is the Boltzmann constant =1.38×10^{-23} J/K, h is the Planck's constant = 6.626×10^{-34} Js, and c is the velocity of light = 2.998×10^{14} μm/s); □□is the□land surface emissivity.

2.4. LULC classification

LULC cartography was produced from the images with TOA reflectance values for 2007 and 2020. Training polygons were created according to the following classes: water body, farmland, urban area, bare soil, forest, grassland, other vegetation (mesquite and arbustive vegetation) and scrubland. A supervised classification was performed in the ENVI 5.3 program using the training polygons, applying the neural network algorithm. Subsequently, the validation of results was carried out through a confusion matrix analysis, which was useful to estimate the classification accuracy degree. Validation required the use of the base cartography of land use and vegetation series VI map developed by INEGI [14].

2.5. LST variation

The variations of LST and its relationship with LULC were evaluated through the quantification of the changes in LULC. The use of a change matrix was fundamental to represent the dynamics of LULC changes in the analyzed periods. Change rate can be calculated according to the following equation 9 [18]:

$$t = \left[\left(\frac{V_2}{V_1}\right)^{\frac{1}{n}} - 1\right] \times 100 \qquad (9)$$

Where for LULC change rate, t is the change rate (%) for each category per year; V_1 corresponds to the area of a LULC category at the beginning year; V_2 is the area of a LULC category at the end year; n is the number of years spanning the period analyzed. Moreover, in the LST change rate, V_1 is the LST value at the beginning year; and V_2 is the LST value at the end year.

3. Result and Discussion

3.1. Distribution and change analysis of LST

LST was obtained from data from the Landsat 8 TIRS and Landsat 5 TM sensors, and a single-channel algorithm was applied. The LST analysis was performed for two seasons; winter and spring. Figure 2 shows the LST values for February and May of 2007. During February, an average LST of 22.19 °C was observed. The highest temperatures are located in the north and southeast of the basin. While in the southern part are located the lowest temperatures. In the case of LST for May, a considerable increase in LST values can be observed, since maximum temperatures of 41.49 °C are recorded, which are concentrated in the central portion of the basin. Also, average LST in this area was 32 °C, representing an increase of 9.18 °C in the average temperature between the analyzed dates.

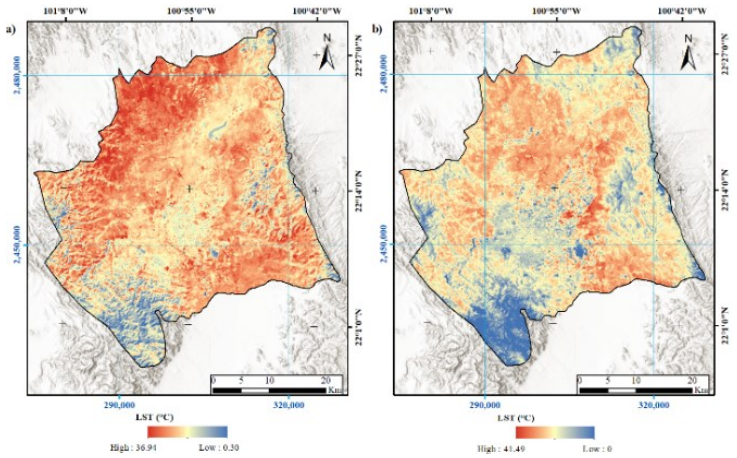

Figure 2. (a) LST distribution of February 2007; (b) LST distribution of May 2007

In figure 3, the distribution of LST for 2020 is indicated. In March, maximum temperatures of 47.71 °C were located in the North and East region of the basin, while minimum temperatures are present in the South and West of the basin. In addition, an average temperature of 34.8 °C was observed. In May, the maximum temperature obtained was 51.44 °C, which can be detected in the eastern central and northern portion of the study area. On this month, the average temperature in the SLPB was 42.28 °C, which represents an increase of 7.48 °C between the two dates analyzed for 2020.

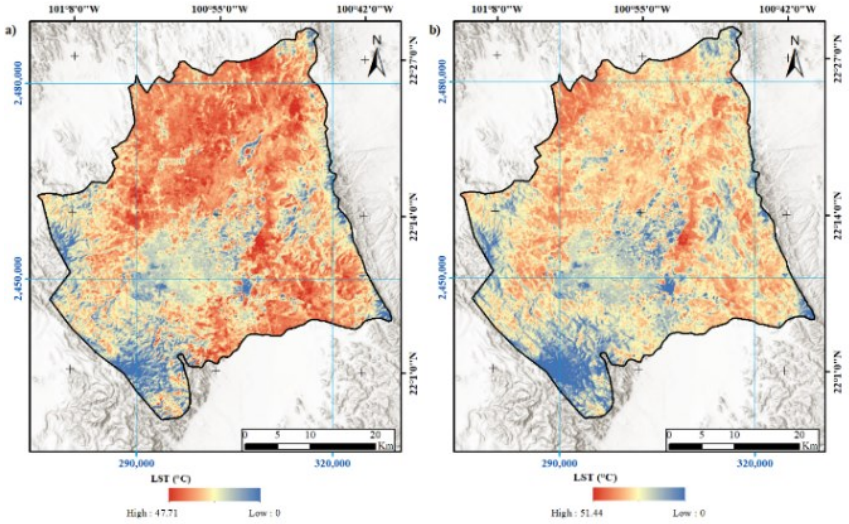

Figure 3. (a) LST distribution of March 2020; (b) LST distribution of May 2020

Based on the results obtained, rate change was calculated for LST values between 2007 and 2020. Table 3 shows the rates change for the winter and spring season of the 2007-2020 period. In winter, an increase in temperature of 0.04 °C per year is recorded, while in spring temperature increased 0.02 °C per year. According to average LST values for winter and spring of 2007-2020, an average LST of 27.10 °C was detected for 2007 and 38.54 °C for 2020, which indicates that there is an average increase of 0.03 °C/year in temperature. This increase shows a constant behaviour, exhibiting a slight increase in the spring season since according to INEGI [19] the highest temperatures for the area are registered during May. Similar results to this study were reported by Pal & Ziaul (2017) [6] in India, where it was found that there are significant changes in LST by each season of the year. However, it is important to analyze the LST behaviour according to LULC, allowing to know how the temperature varies concerning the station and land use.

Table 3. LST rate change in winter and spring for 2007-2020

Season	Average LST (°C)		t (°C)	
	2007	**2020**	**2007**	**2020**
Winter	22.19	34.80	0.04	-
Spring	32.00	42.28	-	0.02

3.2. *LULC changes*

LULC mapping was obtained from remote sensing data, and a supervised classification process was carried out, applying a neural network algorithm. Figure 4 shows the maps obtained from LULC, which were validated using base mapping derived from INEGI [14]. In 2007 classification, the overall precision achieved was 98.27%, and kappa index was 0.97. For the classification of 2020, the overall accuracy was 98.23%, and kappa index was 0.97. According to results, between 2007 and 2020, the urban area growth can be observed; this behaviour was also reported in the study elaborated by

Amuzurrutia-Valenzuela et al. (2015) [20]. As regards other covers, a gradual change was found, the other type of vegetation changed to scrub or grassland, even dense cover vegetation, such as forest, has lost area. Miranda-Aragón et al. (2013) [21] reported similar behavior for the period of 1993-2007.

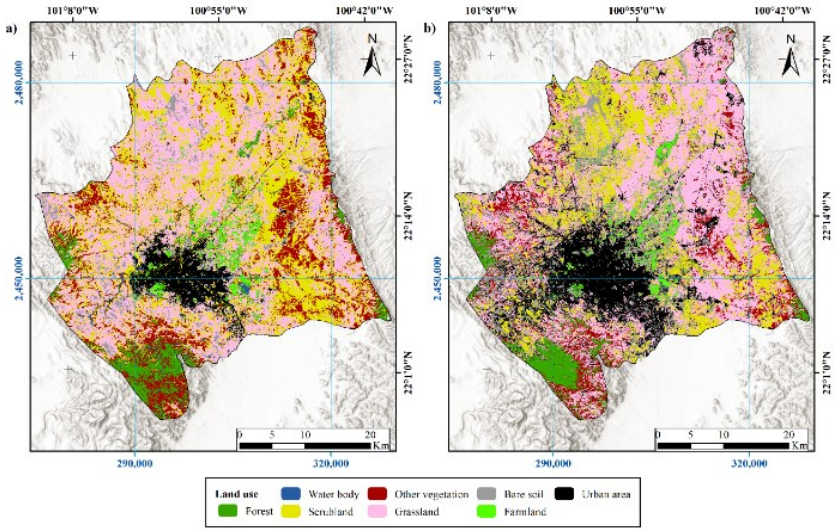

Figure 4. (a) Land Use/Land Cover map of 2007; (b) Land Use/Land Cover map of 2020.

Table 4 indicates the LULC change rates in the 2007-2020 period. According to results obtained, in forest category showed a loss of 1.76% (0.017 km^2/year), which results in a total loss of 21.46 km^2 in the thirteen years elapsed. For water bodies, an annual loss of 0.13 km^2 (13%) was recorded, representing one of the most drastic changes during 2007-2020, since 7.19 km^2 were lost in total. 187.38 km^2 of scrubland decreased, with a change rate of 0.03 km^2/year (3.41%). Likewise, resulting in a rate change of -4.02% for other vegetation, which represents a decrease of 0.04 km^2/year and a total loss of 99.5 km^2 of its original area. As regards grassland, an annual reduction of 0.05% of the total area was observed, losing only 5.17 km^2 in 13 years. In the case of bare soil, a considerable increase was detected (0.08 km^2/year), where mostly coverings such as scrubland, grassland and water bodies changed to bare soil, increasing 141.16 km^2. The irrigated farmland had a slight increase of 0.003 km^2 annually. Finally, the urban area doubled in size with a change rate of 0.07 km^2/year (7.82%/year), which represents a total increase of 178.74 km^2.

Table 4. LULC change rates 2007-2020

LULC category	Area km^2		t (%)
	2007	2020	
Forest	104.12	82.65	-1.76
Water body	8.42	1.23	-13.77
Scrubland	515.96	328.58	-3.41
Other vegetation	240.80	141.25	-4.02
Grassland	703.17	698.00	-0.06
Bare soil	75.47	216.64	8.45
Farmland	30.49	31.98	0.37
Urban area	107.54	286.28	7.82

3.3. *LULC influence on LST*

Zonal statistics were elaborated to analyze LULC influence on LST, where mean LST value was obtained for each LULC category in the analyzed period. In addition, change rates of LST were calculated to characterize coverages that present the most drastic changes in LST. In 2007, LULC categories showing the highest average temperatures, both in winter and summer, are grassland, scrubland, bare soil and urban area, with average LSTs between 22 °C-23 °C for winter and 30°C -33 °C for spring. Meanwhile, the lowest temperatures correspond to covers with dense vegetation such as the forest, and also water bodies showed average LSTs between 17°C -19 °C for winter and 24°C -27 ° C for spring. Further, in general, an LST increase of approximately 10 °C is observed for scrub and grassland between the two seasons studied. In the case of bare soil, other vegetation and urban areas, there is an increase of approximately 9 °C between seasons. For forest, water body, and farmland categories, the temperature increase between seasons was around 8 °C.

In 2020, significant increases in temperature were recorded. Similar to the results obtained for 2007, the LULC categories with the highest LST values are grassland, scrub, bare soil and urban area. For winter, average LST was between 30°C to 34 °C, while for spring average LST values were between 41°C to 45 °C. LST ranges from 20°C to 21 °C for winter and between 30 °C to 32 °C for spring were obtained in covers such as other vegetation and farmland. Also, the lowest mean values of LST were presented in categories such as forest and water bodies with ranges between 17 °C to19 °C for winter and 24°C to 27 ° C for spring. In this year, a constant increase of approximately 8 °C in LST was observed between seasons for each LULC categories, except for water bodies, showing an increase of roughly 3 °C from winter to spring.

Finally, throughout the calculation of change rates for LST in the period 2007-2020, it was detected that the most significant changes in LST per year were obtained in winter for covers such as water bodies (0.042 °C/year), scrubland (0.039 °C/year) and other vegetation (0.037 °C/year). Meanwhile, in the remaining categories, change recorded had a constant behaviour (0.030 °C/year to 0.035 °C/year). As regards spring season, between 2007 and 2020, the annual change in temperature was more constant for all the LULC classes (between 0.020 °C/year to 0.025 °C/year).

In the area of study, similar analyses have not been performed to compare this study regarding others. However, based on results attained in international researches, related behaviours have been reported, and more importantly, it has been observed that in LULC categories where there is no a dense cover of vegetation, LST values are higher [2] [6] [22].

Table 5. Zonal statistics and change rates of LST with respect to LULC

LULC category	Mean LST (°C)				t (°C)	
	2007		2020		2007-2020	
	Winter	Spring	Winter	Spring	Winter	Spring
Forest	18.61	26.55	28.95	36.37	0.035	0.025
Water body	16.99	24.28	29.11	31.58	0.042	0.020
Scrubland	22.63	32.92	37.29	44.49	0.039	0.023
Other vegetation	20.10	29.71	32.38	40.24	0.037	0.024
Grassland	23.29	33.35	35.65	43.04	0.033	0.020
Bare soil	22.84	32.76	34.89	42.33	0.033	0.020
Farmland	20.66	29.52	30.10	38.36	0.029	0.020
Urban area	21.54	30.66	33.29	41.09	0.034	0.023

4. Conclusion

The temporal study carried out in the SLPB allowed addressing the degree of influence that LULC has on LST. Changes observed in LULC during 2007-2020 (13 years), helped to demonstrate that replacement of vegetated surfaces by impervious surfaces has altered the climate of the region since

the forest had a loss of about 20% of its original area (2007). Cover of vegetation (other vegetation) had lost more than 40% of its territory. Analysis performed in winter and spring revealed the existence of seasonal LST variations of approximately 9 °C for both years. The results indicate that from 2007 to 2020, the LST increased from 27.10 °C to 38.54 °C. However, the highest temperatures were recorded in zones where spare vegetation is located (scrubland and grassland) or vegetation is absent (bare soil and urban area). The lowest temperatures were obtained in forest and water bodies. On that basis, it is inferred that spaces with dense vegetation and water have function as regulators of LST.

Remote sensing has proven to be a useful tool for LST retrieval and LULC generation, where the application of the single-channel algorithm and supervised classification methods in Landsat images are valuable and straightforward processes, generating precise and extensive spatial coverage results. However, the use of indicators such as the intensity of land use to determine the level of correlation between LST and LULC, and a full seasonal analysis are suggested for future researches. The results obtained allow to delineate the effects produced on LST by LULC, which are crucial to address the impacts affecting the climate balance of the region. This type of analysis is useful to improve climate change mitigation measures through an improvement in land use planning systems.

References

[1] Mujabar P S 2019 Spatial-temporal variation of land surface temperature of Jubail Industrial City, Saudi Arabia due to seasonal effect by using Thermal Infrared Remote Sensor (TIRS) satellite data *Journal of African Earth Sciences* **155** 54-63. https://doi.org/10.1016/j.jafrearsci.2019.03.008

[2] Bharath S, Rajan K S & Ramachandra T V 2013 Land surface temperature responses to land use land cover dynamics. *Geoinfor Geostat: An Overview* **54** 50-78. http://dx.doi.org/10.4172/2327-4581.1000112

[3] Schuch F, Marpu P, Masri D & Afshari A 2017 Estimation of Urban Air Temperature from a Rural Station Using Remotely Sensed Thermal Infrared Data. *Energy Procedia* **143** 519-525. https://doi.org/10.1016/j.egypro.2017.12.720

[4] Avdan U & Jovanovska G 2016 Algorithm for automated mapping of land surface temperature using LANDSAT 8 satellite data. *Journal of Sensors*, 2016. https://doi.org/10.1155/2016/1480307

[5] Kuang W, Li Z & Hamdi R 2020 Comparison of surface radiation and turbulent heat fluxes in Olympic Forest Park and on a building roof in Beijing, China. *Urban Climate* **31** 100562. https://doi.org/10.1016/j.uclim.2019.100562

[6] Pal S & Ziaul S K 2017 Detection of land use and land cover change and land surface temperature in English Bazar urban centre. *The Egyptian Journal of Remote Sensing and Space Science* **20** (1) 125-145. https://doi.org/10.1016/j.ejrs.2016.11.003

[7] Haylemariyam M B 2018 Detection of Land Surface Temperature in Relation to Land Use Land Cover Change: Dire Dawa City, Ethiopia. *J Remote Sens GIS* **7** 245. https://doi.org/10.4172/2469-4134.1000245

[8] Xiao H, Kopecká M, Guo S, Guan Y, Cai D, Zhang C & Yao W 2018 Responses of urban land surface temperature on land cover: A comparative study of Vienna and Madrid. *Sustainability* **10** 2 260. https://doi.org/10.3390/su10020260

[9] Alam A, Bhat M S & Maheen M 2019 Using Landsat satellite data for assessing the land use and land cover change in Kashmir valley. *GeoJournal*. https://doi.org/10.1007/s10708-019-10037-x

[10] Gogoi P, Vinoj V, Swain D et al 2019 Land use and land cover change effect on surface temperature over Eastern India. *Sci Rep* **9** 8859. https://doi.org/10.1038/s41598-019-45213-z

[11] Jiang J & Tian G 2010 Analysis of the impact of land use/land cover change on land surface temperature with remote sensing. *Procedia environmental sciences* **2** 571-575. https://doi.org/10.1016/j.proenv.2010.10.062

[12] Diario Oficial de la Federación 2010 Acuerdo por el que se dan a conocer los estudios técnicos

del acuífero 2411 San Luis Potosí, en el Estado de San Luis Potosí. México, edición del 7 de julio.
[13] U S Geological Survey 2018 online: https://earthexplorer.usgs.gov/
[14] INEGI 2016 Conjunto de datos vectoriales de Uso del suelo y vegetación. Escala 1:250 000. Serie VI. Edición: 2016. Febrruary 1, 2019, de *Instituto Nacional de Estadística y Geografía (INEGI)*. Online: https://www.inegi.org.mx/app/biblioteca/ficha.html?upc=889463173359
[15] Chander G, Markham B L & Helder D L 2009 Summary of current radiometric calibration coefficients for Landsat MSS, TM, ETM+, and EO-1 ALI sensors. *Remote sensing of environment*, **113** (5) 893-903. https://doi.org/10.1016/j.rse.2009.01.007
[16] Arizza A 2013 Descripción y Corrección de Productos LandSat 8 LDCM (LandSat Data ContinuityMission) Versión 1.0. Centro de Investigación y Desarrollo en Información Geográfica (CIAF), *Instituto Geográfico Agustín Codazzi (IGAC), Colombia*.
[17] Van de Griend A & OWE M 1993 On the relationship between thermal emissivity and the normalized difference vegetation index for natural surfaces. *International Journal of remote sensing*, **14** (6) 1119-1131. https://doi.org/10.1080/01431169308904400
[18] Organización de las Naciones Unidas para la Alimentación y la Agricultura 1996. Forest resources assessment 1990. *Survey of tropical forest cover and study of change processes*. FAO. Roma.
[19] INEGI Cuéntame, Información por entidad – San Luis Potosí. May 15, 2020, de *Instituto Nacional de Estadística y Geografía (INEGI)*. online: http://cuentame.inegi.org.mx/monografias/informacion/slp/territorio/clima.aspx?tema=me&e=24
[20] Amuzurrutia-Valenzuela D, Aguirre-Salado C & Sánchez-Díaz G 2015 ¿Hacia dónde crecerá la ciudad de San Luis Potosí (México) después de 2009?. *Eure (Santiago)* **41** (124), 113-117. http://dx.doi.org/10.4067/S0250-71612015000400006
[21] Miranda-Aragón L, Treviño-Garza E J, Jiménez-Pérez J, Aguirre-Calderón O A, González Tagle M A, Pompa-García M & Aguirre-Salado C A 2013 Tasa de deforestación en San Luis Potosí, méxico (1993-2007). *Revista Chapingo serie ciencias forestales y del ambiente*, **19** (2) 201-215. http://dx.doi.org/10.5154/r.rchscfa.2011.06.044
[22] Sun Q, Wu Z & Tan J 2012 The relationship between land surface temperature and land use/land cover in Guangzhou, China. *Environmental Earth Sciences*, **65** (6) 1687-1694. https://doi.org/10.1007/s12665-011-1145-2